Preliminary simulation studies on a cylindrical PEM scanner using GATE*

YAN Qiang(闫强)[1,2] GAO Juan(高娟)[1,2] SHAN Bao-Ci(单保慈)[1;1)] WEI Long(魏龙)[1]

[1] Key Laboratory of Nuclear Analysis Techniques, Institute of High Energy Physics, Chinese Academy of Sciences, Beijing 100049, China
[2] Graduate University of Chinese Academy of Sciences, Beijing 100049, China

Abstract In this paper, we investigate the performance of a cylindrical positron emission mammography (PEM) by simulation, in order to estimate its feasibility before implementation. A well-developed simulation package, Geant4 Application for Tomographic Emission (GATE), is used to simulate the scanner geometry and physical processes. The simulated PEM scanner is composed of 64 blocks axially arranged in 4 rings with an axial field-of-view (AFOV) of 12.8 cm and 16.6 cm in diameter. For each block, there is a 16×16 array of 2 mm×2 mm×15 mm lutetium yttrium oxyorthosilicate (LYSO) crystals. In the simulated measurements, the spatial resolution is at the center of the FOV of 1.73±0.07 mm (radial) and 1.81±0.08 mm (tangential), but of 4.83±0.09 mm (radial) and 4.37±0.07 mm (tangential) while 5 cm off the center. The central point source sensitivity (ACS) is 4.04% (1.50 Mcps/mCi) at an energy window of 350–650 keV. Moreover, the capillary and cylindrical sources are simulated coupled to breast phantoms for the scatter fraction (SF) and Noise Equivalent Count Rate (NECR) test. For a breast phantom with a 350–650 keV energy window, SF may reach the highest 32.95%, while NECR is degraded down to the lowest 255.71 kcps/mCi. Finally, we model a breast phantom embedded with two spheres of different activities. The reconstructed image gives good results despite a bit of difference in image contrast. Further, the image quality will be improved by scatter and random correction. All these test results indicate the feasibility of this PEM system for breast cancer detection.

Key words simulation, GATE, cylindrical PEM, evaluation

PACS 87.55.kh, 87.57.uk, 87.57.␣s

1 Introduction

Early stage breast cancer detection has become a current trend in nuclear medical imaging research. As a non-invasive technique, the positron emission imaging technique has been effectively applied to the detection of breast cancer. The first positron emission mammography (PEM) scanner was proposed in 1994 by Thompson et al [1], and consists of two opposite detector arrays above and below the breast. To achieve high sensitivity and good spatial resolution, one new generation of dedicated positron emission scanners after another has been investigated [2–5]. Finally, Weinberg's group [6] worked out the first commercial breast imaging scanner consisting of two sets of planar detectors. All these PEM systems have two static planer detectors, so the limited-angle tomography leads to the image blurring along the axis perpendicular to the planes of the detectors. To solve this problem, the multi-center mode [7] and rotating detector arrays [8, 9] were recently proposed and well studied. Otherwise, a simulated investigation finds that the cylindrical PEM system has better spatial resolution and noise effective count rate (NECR) for breast imaging, compared with whole-body PET [10]. Though the cylindrical PEM system has good performances as mentioned, it has not become commercial. An "863" project was developed for research and development of the PEM system. Considering the imperfect sampling of the planner PEM system, a cylindrical PEM system was proposed for breast cancer detection. The objective of this work is to find out whether the design of this cylindrical PEM system satisfies the anticipative requirements in the

Received 2 March 2009, Revised 17 March 2009
* Supported by National High-tech Research and Development Program of China (863) (2006AA020803)
1) E-mail: shanbc@ihep.ac.cn

project. The detailed performances of the cylindrical PEM scanner are studied by simulation.

The software used for simulation here is Geant4 Application for Tomographic Emission (GATE), which is a powerful research tool developed for nuclear medicine imaging applications, e.g. for Positron Emission Tomography (PET) and Single Photon Emission Computed Tomography (SPECT) simulations [11–12]. The validation of GATE for the simulation of different clinical and small animal PET systems has been well studied [13–15]. In this paper, GATE is used to model the cylindrical PEM prototype for evaluating the performance protocols including spatial resolution, sensitivity, Noise Equivalent Count Rate (NECR), scatter fraction (SF) and so on.

2 Material and methods

The GATE simulation platform was developed in 2001, and has the capability to precisely and efficiently model physics phenomena, complex detector designs, phantoms and source distribution. The global architecture of GATE has been described in detail [16, 17]. In this work, the photoelectric effect, Compton scattering, and Raleigh scattering are taken into account. All simulated experiments have a coincidence timing window of 6 ns and an energy resolution of 20%. The simulated LYSO-based PEM camera (Fig.1) consists of 4 detector rings of 16 flat blocks. Each block is built with a 16×16 array of 1.9 mm × 1.9 mm × 15 mm LYSO crystals with a 2.0 mm crystal pitch. Therefore, the scanner design results in an axial field of view (FOV) of 12.8 cm and a radial FOV of 11.2 cm.

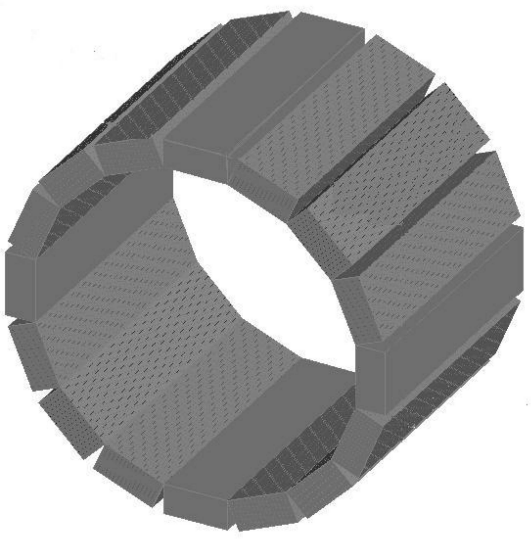

Fig. 1. Illustration of the simulating PEM scanner.

Because there are currently no published testing standards for breast PEM scanners, we synthesized the earlier literature articles reporting the performances of breast PEM scanners, small-animal PET scanners and whole-body human PET scanner to propose a testing protocol. The four parts mentioned in this protocol are spatial resolution, sensitivity, scatter fraction (SF) and NEC rates, as well as the image quality of a breast phantom. According to the NIMA protocol [18] and Ref. [19], we designed the proper simulation time to get enough event counts. In our simulations, coincidences were collected to ensure that the statistical requirement is satisfied.

2.1 Spatial resolution

According to the reference of the spatial resolution measure of PEM/PET [9], the transaxial spatial resolution of the camera was tested by imaging a series of capillary tubes along the vertical direction of the scanner. The capillary tube sources, filled with ^{18}F (1 μCi) which were 0.5 mm in radius and 12.8 cm in length, were positioned perpendicularly and horizontally at the center, 1.0 cm, 2.5 cm and 5.0 cm away from the center and along the axis of the scanner. 3D data were acquired for 3 min, and then reformed to 2D sinograms with the single-slice rebinning algorithm (SSRB) and Fourier rebinning (FORE) methods. Then, the image was reconstructed with the 2D Filtered Backprojection (FBP) method with ramp filter, and the FWHM values were calculated. Here an energy window of 350 to 650 keV was used.

2.2 Sensitivity

Sensitivity is defined as the proportion of the detected coincidence counts to the total counts emitted by the source. Here axial sensitivity profile [18] and absolute central point source sensitivity (ACS) were measured by simulation. A 0.5 mm radius point source of ^{18}F (1.11 kBq [30 μCi]) was located in the center of the FOV and transferred in steps of 1.0 mm all over the entire axial field of view. As the source was surrounded by a 1.0 mm radius spherical plastic phantom, attenuation effects were neglected. According to the NEMA protocol, the source was scanned for 30 s at each position to ensure that at least 10000 true coincidences per slice are collected. The coincidence count rates were measured for 1.0 s at each step in three energy windows of 400–600, 350–650, and 250–750 keV, all of which were plotted in the axial sensitivity profile. ACS values were the coincidence count rates of the point source in the center of the transverse and axial directions.

2.3 Scatter fraction (SF) and NEC rates

The phantom located in the center of the FOV was simulated with a cylinder of 8.0 cm in diameter and 12.8 cm in length, filled with water and breast separately in two testing conditions. The ^{18}F source contained an initial activity of 30 μCi which fully filled the phantom; in another condition, a 1.0 mm diameter capillary of 12.8 cm long was located 2.0 cm away from the center of the FOV. Therefore, two kinds of phantoms cooperating with two kinds of sources lead to four situations, which were used for scatter fraction (SF) and NEC rate measurements in different energy windows of 400–600, 350–650, and 250–750 keV. They were calculated according to these formulas:

$$SF = \frac{S}{T+S+R}, \tag{1}$$

$$NECR = \frac{T^2}{T+S+kR}, \tag{2}$$

where T is the true coincidence rate, S the scattered coincidence rate, R the random coincidence rate, and k is the diameter of the phantom divided by the diameter of the effective field of view, which equaled 0.71 for the breast phantom. The data in each condition were collected for 20 min to obtain enough coincidence counts, in order to satisfy the requirements of the NIMA protocol [18].

2.4 Breast lesion model test

In order to investigate the performance of the cylindrical PEM system the detecting small breast lesions, two 5.0 mm diameter spheres were placed in a cylindrical breast phantom of 8.0 cm in diameter. The breast phantom was filled with 30 μCi ^{18}F, and the two spheres and phantom were separately filled with different activities of ^{18}F radioactivity. The activity ratio of the left sphere to the surrounding breast background was 7:1, while that of the right sphere was 3:1. The distance between two sphere centers was 7.0 mm. This experiment was supposed to evaluate the quality of the breast image by simulation. Commonly, the breast is scanned for 10 min in real PEM detection. But for the phantom study, we spent more time to obtain enough coincidence counts. We set the simulation time according to the time used in animal-PET [19], which has a similar structure to the scanner and a similar size to the phantom. The image data were collected for 20 min. The energy window and FBP parameters were the same as in Section 2.1.

3 Results

3.1 Spatial resolution

A transaxial image of capillary sources is shown in Fig. 2. Note that a similar distribution of point sources is found in the horizontal and perpendicular positions. The same result is also revealed by the average radial and tangential spatial resolution (mean±SD) measured with the full-width-at-half maximum (FWHM) of different axial positions in Table 1. The spatial resolution in the center of the FOV reaches 1.73 mm, but drops approximately down to 4.83 at the 5.0 cm offset, mainly due to the effect of depth of interaction.

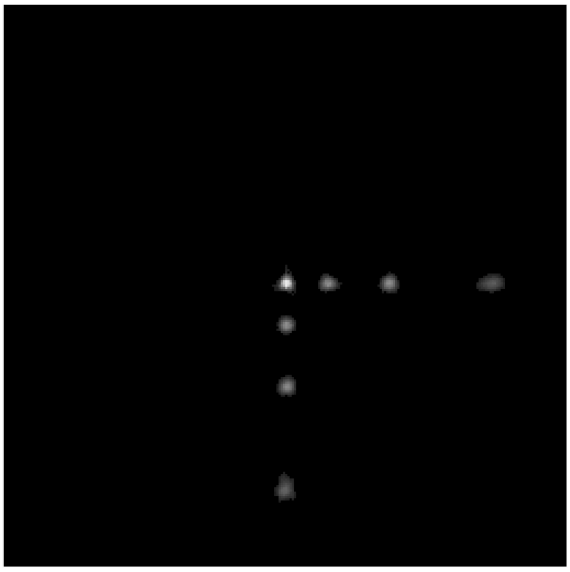

Fig. 2. Representative transaxial PEM image of the capillary tube phantom used to measure the radial and tangential components of spatial resolution.

Table 1. Average spatial resolution results measured at axial offset from the center of the scanner.

	distance from the center of the scanner/cm			
	0.0	1.0	2.5	5.0
radial resolution/mm	1.73 ±0.07	2.54 ±0.08	2.85 ±0.05	4.83 ±0.09
tangential resolution/mm	1.81 ±0.08	2.75 ±0.07	3.02 ±0.06	4.37 ±0.07

3.2 Sensitivity

For the cylindrical PEM, absolute sensitivity of three different energy windows is plotted against the total axial positions in Fig. 3. This profile is symmetrical and triangular, and the maximum absolute sensitivity is found at the center of the AFOV, as

listed in Table 2. The ACS of 400–600, 350–650, 250–750 keV energy windows is 3.75%, 4.04% and 6.37% respectively, which demonstrates a good detection efficiency.

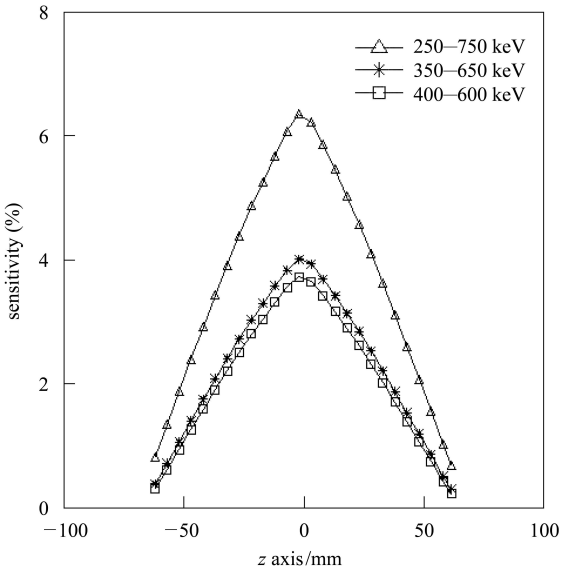

Fig. 3. Absolute sensitivity curves for three different energy windows.

Table 2. ACS values and coincidence count rates for different energy windows.

energy window/keV	ACS (%)	coincidence count rate/(Mcps/mCi)
400–600	3.75	1.39
350–650	4.04	1.50
250–750	6.37	2.36

3.3 SF and NEC rates

The SF and NEC rates for cylindrical and capillary sources in breast and water phantoms respectively were simulated at three energy windows around 511 keV in Table 3. Comparison between the breast and water phantom results shows that the breast phantom of higher density has a higher SF and a lower NECR as estimated. In another aspect, the off-center source model has a more serious scatter effect and lower effective count rates, compared with the source of uniform distribution.

Table 3. Scatter fractions and NEC rates.

phantom	cylindrical source				capillary source			
	breast		water		breast		water	
energy window/keV	SF (%)	NECR/ (kcps/mCi)	SF (%)	NECR/ (kcps/mCi)	SF (%)	NECR/ (kcps/mCi)	SF (%)	NECR/ (kcps/mCi)
400–600	21.57	305.25	21.39	308.31	24.53	256.30	24.24	261.34
350–650	29.22	311.85	28.99	315.38	32.95	255.71	32.60	261.40
250–750	41.05	387.48	40.72	392.66	45.39	306.09	44.90	313.49

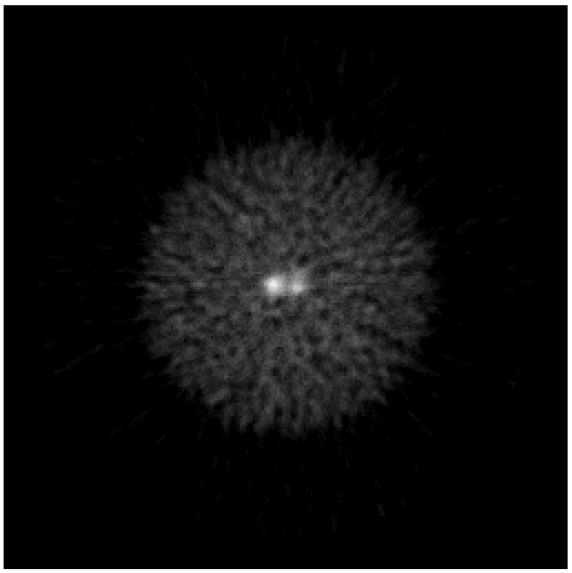

Fig. 4. Transverse slice of PEM-breast lesion image reconstructed with the FBP method and attenuation correction.

3.4 Breast lesion model test

Figure 4 displays a transverse FBP image of the cylindrical breast phantom, with good agreement with the simulated configuration. The phantom contains two simulated FDG-avid lesion spheres of 5.0 mm in diameter. The left-to-right ratio is calculated as the quotient of the two mean values of round areas in the center slice of the image. Compared with the ideal ratio 2.33, the simulated result of the ratio is equal to 1.47. The main reason for the smaller ratio may lie in the fact that this reconstructed image does not have accurate scatter and random correction. In addition, the FBP and rebinning methods may also bring error into the reconstructed image.

4 Discussions

In this work, a cylindrical PEM system was simu-

lated to assess whether it was sufficient for breast lesion imaging. The simulated investigation for the evaluation of the PEM scanner performance was based on a number of protocols referring to those of body-PET, animal-PET and planar breast PEM. The result showed that spatial resolution was good at the center of the FOV, but somewhat degraded off the center due to the DOI effect. The tests of sensitivity, SF and NECR also produced good results. In particular, an image quality phantom of a cylindrical breast containing two spherical lesions was studied to investigate lesion detection ability. Good reconstructed image quality except a little bad image contrast is revealed in Fig.4, which supports the view that the PEM mentioned above is a promising system for breast imaging. Compared to the latest planer PEM [9], the sensitivity (6.88%) of the planer PEM is 1.7 times as high as the sensitivity (4.04%) of the cylindrical PEM. That is because the amount of crystals in the planer PEM is 1.7 times as many as that in the cylindrical PEM, although they use a LYSO crystal pixel of the same size. So if we suppose that the planar PEM has the same amount of crystals as the cylindrical PEM, the sensitivity of the planar PEM (4.07%) is almost equivalent to that of the cylindrical PEM, which is computed approximately according to the solid angle relationship. At the center of the FOV, the spatial resolution of the cylindrical PEM can reach 1.73 mm, better than the 2.01 mm of the planer PEM. But offset from the center, the spatial resolution (4.83 mm) of the cylindrical PEM degrades more due to the DOI effect, compared to the steady spatial resolution (2.11 mm) in the planer PEM. According to the structure of the planer PEM, there are still coincidence events without the DOI effect offset from the center of FOV. Therefore in the planar PEM, only these coincidence events, whose DOI effect is not serious, are used for reconstruction to avoid degradation of the spatial resolution. This planar PEM is rotated to get complete sampling of the angle, which leads to complexity in the manufacture. In addition, the crystals used in this planar PEM are 1.7 times as many as in the cylindrical PEM. That is, this planar PEM increases the costs and complexity of the manufacture.

In tests, the dead time and the efficiency differences of different crystals are also important parameters, but they are ignored in our above-mentioned simulations. This is because they are dependent on the characteristics of the device. To approach a real situation, the simulation should include dead time and efficiency parts in future research.

In short, compared with a planar PEM with the same amount of crystals, the cylindrical PEM has better spatial resolution at the center of the FOV and equivalent sensitivity, in spite of the modest bad spatial resolution off the center of the FOV. So synthetically, considering the costs and complexity of manufacture in addition to the performance of the two kinds of PEM systems, we choose the cylindrical PEM system in our real manufacture. After initial testing of the cylindrical PEM system, we confirm that this cylindrical PEM system is basically suited to breast lesion imaging.

References

1 Thompson C J, Murthy K, Weinberg I N et al. Med. Phys., 1994, **21**: 529–38
2 Rosen E L, Turkington T G, Soo M S et al. Radiology, 2005, **234**: 527–34
3 Doshi N K, SHAO Y, Silverman R W et al. Med. Phys., 2000, **27**: 1535–43
4 Raylman R R, Majewski S, Wojcik R et al. Med. Phys., 2000, **27**: 1943–54
5 Motta A, Righi S, Del Guerra A, Belcari N et al. Methods Phys. Res. A, 2004, **527**: 201–5
6 Weinberg I N, Beylin D, Zavarzin V et al. Cancer Res. Treat, 2005, **4**: 55–60
7 Berg W A, Weinberg I N, Narayanan D et al. The Breast J, 2006, **12**: 309–23
8 Raylman R R, Majewski S, Kross B et al. Nucl. Instrum. Methods Phys. Res. A, 2006, **564**: 291–5
9 Raylman R R, Majewski S, Smith M F et al. Physics in Medicine and Biology, 2008, **53**(3): 637–653
10 Karimian A, Thompson C J, Sarkar S et al. Nuclear Instruments and Methods in Physics Research A, 2005, **545**: 427–435
11 http://opengatecollaboration.healthgrid.org/
12 Jan S, Santin G, Strul D et al. Phys. Med. Biol., 2004, **49**: 4543–61
13 Lazaro D, Buvat I, Loudos G et al. Phys. Med. Biol., 2004, **49**: 271–285
14 Schmidtlein C R, Kirov A S, Bidaut L M et al. Med. Phys., 2006, **33**: 198–208
15 Gonias P, Bertsekas N, Liaparinos P et al. Nucl. Instr. Meth. Phys. Res. 2007, **571**: 263–266
16 Santin G, Strul D, Lazaro D et al. IEEE Trans. Nucl. Sci., 2003, **50**: 1516–1521
17 Strul D, Santin G, Lazaro D et al. Nucl. Phys. B (Proc. Suppl.), 2003, **125**: 75–79
18 Rosslyn. VA: National Electrical Manufacturers Association; 2001. Standards Publication NU 2-2001
19 WANG Yu-Chuan, Jurgen Seidel, Benjamin M W Tsui et al. Juan J. J Nucl. Med., 2006, **47**: 1891–1900